Engineering Structures 173 (2018) 908–917

Contents lists available at ScienceDirect

Engineering Structures

journal homepage: www.elsevier.com/locate/engstruct

Nonlinear behavior of single bolted flange joints: A novel analytical model

Farhad Meisami, Majid Moavenian*, Aref Afsharfard

Mechanical Engineering Department, Engineering Faculty, Ferdowsi University of Mashhad, Mashhad, Iran

ARTICLE INFO

Keywords:
Flange joint
Bending stiffness
Bilinear behavior
Natural frequencies
Experimental study

ABSTRACT

Flange joints are widely used in mechanical and civil structures. In this study joint deformations are investigated and a detailed model, which can demonstrate the actual joint behavior, is developed. This is done by modeling joint laps and bolts respectively as cantilever beams and springs. Then, an accurate relation between their load and deflection is obtained. It is shown that unlike the lap joints, the flange joints should be modeled using bilinear stiffness. Furthermore, the Euler-Bernoulli theory is used to model dynamic behavior of the beams, which are connected to the flange joint. An analytical procedure is introduced to calculate natural frequencies and mode shapes of two beams, which are connected by a single bolt flange joint. Two experimental setups consisting of a single bolt flange joint specimen and beam-flange system have been designed to investigate static and dynamic behavior of the system. One of the specimens is put into different loading configurations to obtain moment-slope curve. Another setup, consisting of freely suspended beams connected by a single bolt flange joint, is used to investigate natural frequencies of the system. Comparing the theoretical flange stiffness with the experimental and FEM results shows accuracy of the proposed model. Furthermore, dynamic behavior of the proposed beam-spring model is validated using empirical natural frequencies.

1. Introduction

Mechanical joints like flanges, x-joints, lap joints, etc. are widely used in industrial, aerospace and marine structures [1–4]. Flanges mainly come in circular configuration to connect two bodies by a several number of bolts. They also come in non-circular configuration in order to connect two plates [5,6]. Some of the common applications is in connections of airplane parts, petroleum refinery towers, rocket stages and jet engine casings [7–11].

For simplicity, in order to analyze the dynamic behavior of mechanical systems, joints are generally modeled by equivalent spring and damper. In doing so, stiffness and damping of the equivalent system are empirically obtained [12–14] or numerically calculated [6,15–19]. Identifying these parameters is a fundamental step towards achieving an accurate model of mechanical systems with Flange joints. Although the flange joints have various application, their effects on behavior of the mechanical structures are not well defined and in many applications it is assumed the flange joints are rigid connections [20]. However, the previous researches reveal that this is an over estimated assumption and does not provide a good estimate of the joint characteristics [21].

One of the first studies on flange joints was done by Agatonovic in 1985 [22]. He proposed a finite element model of a pressurized bolted flange. This model consists of a single bolt and its pressurized cone, which considered as beam that lay on the beneath.

Shi et al. introduced a model for analyzing moment-deflection behavior of an endplate connection [23]. They proposed a 6-bolted joint into separate T-shaped single bolt joints and obtained a beam-based model for each of them. The complete model constitutes of separate T-shaped models which were assembled together. Luan et al. presented a simplified nonlinear model for the analysis of pipe structures with bolted flange joints [24]. They segmented the full circular flange into separate single bolt models and extract a bilinear longitudinal spring model for each of them. Schwingshackl et al. investigated the nonlinear dynamic behavior of bolted flange joints in jet engines [6]. They demonstrated that the maximum energy dissipation occurs on bolt flange contact. Wu et al. obtained nonlinear dynamic behavior of bolted flanges under various loadings [18]. They found that despite elastic deformations the system has non-linear behavior due to changes in the contact area between the two edges. Meisami et al. studied static behavior of the flange joint under axial and lateral loadings [25]. They show that the joint has nonlinear behavior under axial and lateral loadings. Several studies are reported also investigating stress and strength of bolted flange joints [26–28] which are not covered by this literature review.

Due to complexity of modeling and analysis of the bolted joints with several bolts in different configurations, the joints generally divided

* Corresponding author.
E-mail address: Moaven@um.ac.ir (M. Moavenian).

https://doi.org/10.1016/j.engstruct.2018.07.035
Received 18 December 2017; Received in revised form 26 June 2018; Accepted 11 July 2018

Nomenclature

A	Cross section area (m^3)
E	Young's modulus (N/m^2)
I	Area module of inertia (m^4)
K	Stiffness (N/m, Nm/rad)
L	Beam length (m)
l	Distance to O (m)
R	Average diameter of the bolt's head (m)
t	Thickness (m)
δ, γ	Deflection (m)
θ, φ	Slope (Rad)
ν	Poisson ratio
ω	Natural frequency (rad/s)

Superscript

+	Positive deformation and slope
−	Negative deformation and slope

Subscript

B	Bolt
fl	Flange
l	Longitudinal
t	Torsional

into separate single bolt sub-sections. In previous studies, which are investigated the multi-bolted joints (lap joints, flanges and endplates) generally the equivalent single-bolted models are considered [11,24,29]. But in case of the single bolt joints most of the investigations are focused on the lap joints. Ahmadian and Jalali [30–32], Iranzad and Ahmadian [33] and Abad et al. [13] investigated the dynamic response of two beams connected by a single bolt lap joint in order to identify dynamic behavior of the joints. The main purpose of these experimental studies is to estimate the damping behavior of the joint.

In this study, a novel theoretical model for the flange joints, which simulates the actual joint behavior, is proposed. Unlike the previous investigations [25], not only the static behavior of the joint is considered but also the dynamic behavior is studied analytically and experimentally. It should be noted that, in this study, the aim is to obtain the dynamic behavior of the beam-joint system, so only deformation properties of the joint are considered and the strength is not concerned. This model helps researchers in this area to obtain more accurate equivalent joint stiffness. Furthermore, a new analytical procedure is introduced to calculate natural frequencies of the mechanical elements which are connected by a single bolt flange joint. Obtaining analytical solution of a problem is important because:

- In comparison with numerical and experimental solutions, it can be more accurate.
- It can facilitate evaluation of mechanical parameters effect on the system.

To achieve this, first, the joint was modeled as cantilever beam and the nonlinear springs were considered to analytically obtain the joint stiffness. Then, assigning appropriate conditions, natural frequencies and mode shape of a system consisting of two beams connected to a single bolt flange joint was extracted. Two test setups were configured to verify the static and dynamic responses of the system. The first one was used to test static moment-slope and verify the analytically obtained joint stiffness. The second setup is used to validate the calculated natural frequencies of the beam-flange system. The novelties of this study include:

- Introducing a new analytical formulation to calculate the stiffness of single bolted flange joints
- Introducing a new equivalent model of a system consisting of two beams connected by a single bolt flange joint
- Introducing a new analytical method to calculate natural frequencies of the system consisting of two beams connected by a single bolted flange joint

2. Material and methods

2.1. Problem statement

This paper focuses on deformations of single bolt flange joints and develops a novel detailed analytical model of the joint structure, which can demonstrate the actual joint behavior. For this purpose, the joint laps are modeled as cantilever beams and the bolt modeled with two longitudinal and torsional springs. Then, an analytical model of a system consisting of two beams connected by a single bolt flange joint is developed using Euler-Bernoulli beam theory having free-free boundary conditions and appropriate compatibility conditions at the center. Finally, natural frequencies of this system are obtained and compared with experimental frequencies.

2.2. Analytical joint modeling

2.2.1. Equivalent model of the flange joint

Unlike the flange joints, in bolt lap connections the bolt is perpendicular to the beam. Because of the bolt lap joint geometrical symmetry, the lateral deflections of the joint under positive and negative moments are the same. Fig. 1 compares the bolt lap and flange lap connections in different lateral deflections. As shown in this figure the lateral deflections of the flange joint under positive and negative moments are different. Therefore, it can be concluded that lateral dynamic behavior of the flange joint can be nonlinear.

For theoretically analyzing, the dynamic and static behavior of the flange joint, it should be simulated using equivalent damping and stiffness. Fig. 2 depicts the equivalent model of the beam-flange system consisting of two beams which are connected by a bilinear torsional and longitudinal springs. The joint behaves differently under positive and negative moments, so the torsional behavior of these joints should be

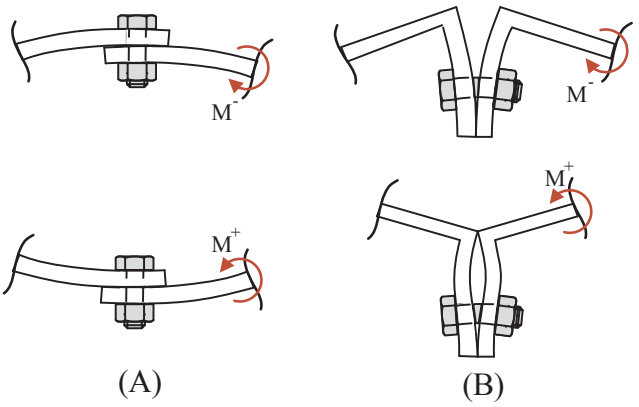

Fig. 1. Lateral behavior of bolt lap (A) and flange lap (B) joints under the positive and negative loadings.

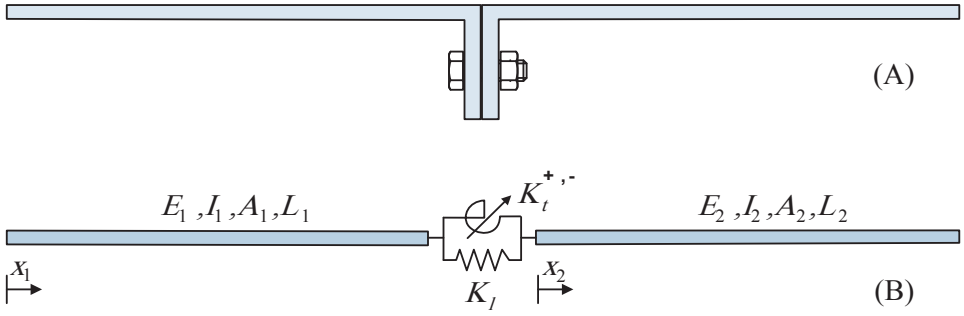

Fig. 2. Schematic of beams connected by single bolt flange joint (A); and equivalent model (B).

described using bilinear springs. It should be noted that in analytical study of the model, the damping properties is not taken into account, because the flange laps have pure rolling motions during opening and closing deformations and these motions are theoretically considered frictionless.

Bending deformations are considered as two separate positive and negative modes (Fig. 1). The loads and deformations that lead to opening and closing the joint edges are respectively named positive and negative loads and deformations. For each of the discussed deformations, a distinct model is proposed that analytically calculates flange deformations with respect to external moment. In other words, the stiffness of the joint can analytically be obtained.

2.3. Analytical calculation of the equivalent stiffness

The positive and negative stiffness of the equivalent bilinear spring should be calculated separately. For this reason, the flange deformations should precisely be observed. Hence, a detailed model including a beam, longitudinal and torsional springs, as shown in Fig. 3, is considered. The longitudinal and torsional springs represent the longitudinal and bending stiffness of the bolt. As far as we know, the main difference between present study and previous investigations can be listed as follows:

- The dynamic behavior of the flange joint is described using nonlinear double spring model.
- Unlike previous studies, which present a simple model for longitudinal behavior of the single bolt joint, this study focuses on the lateral behavior of the joint.
- Distributed loading is considered to present the bolt normal loading.
- A torsional spring is considered to precisely present bending behavior of the bolt.

2.3.1. Positive deformations

Part (A) of Fig. 3 shows a half joint model under positive bending moment. Based on this figure the half flange joint behavior is studied. Because of similarity in geometry and loading of each half, this simplification would be reasonable [14]. As shown in Fig. 3-b, the bolt is replaced with a combination of torsional and longitudinal springs. Fig. 3-c presents the beam loadings model. The bolt loads are shown as an extended tensional load (F_B) and concentrated bending moment (M_B).

When an external moment exerted on the point *O*, (which indicates the inner edge of the flange) the flange laps from O to B are separated. The separation point (*C*) will be away from *B* towards the outer flange edge with increase of moment. The lengths from the inner flange edge (*O*) to the separation point and the bolt location are respectively shown with l_C and l_B. The whole width of the flange also is indicated with l_O.

Because *C* represents the separation point, so the beam part AC remains undeformed. This means that the separated flange lap (OC) can be modeled as a cantilever beam with the length of the l_c. Note that l_c increases with increasing the external load. The aim of the model is to obtain slope of the beam at point O as a function of the external moment. For this purpose, the dimensionless parameter of the separated length (*X*) is defined as follows:

$$X = \frac{l_C - l_B}{l_B} \tag{1}$$

From the equilibrium around point (C) Eq. (2) is determined.

$$F_B X l_B + M_B - M = 0 \tag{2}$$

At the point B, the deflection and slope of the beam (δ_B and θ_B) are respectively equal to the axial deflection and bending angle of the bolt (γ_B and φ_B). This definition is presented in Eqs. (3) and (4).

$$\delta_B(X, F_B, M_B) = \gamma_B(F_B) \tag{3}$$

$$\theta_B(X, F_B, M_B) = \varphi_B(M_B) \tag{4}$$

Fig. 4 depicts the deformation and slope of the bolt and flange at point B. Furthermore, the axial deflection and bending angle of the bolt are functions of F_B and M_B. Therefore, unknown variables *X*, F_B and M_B can be obtained by simultaneously solving Eqs. (2)–(4). Having the

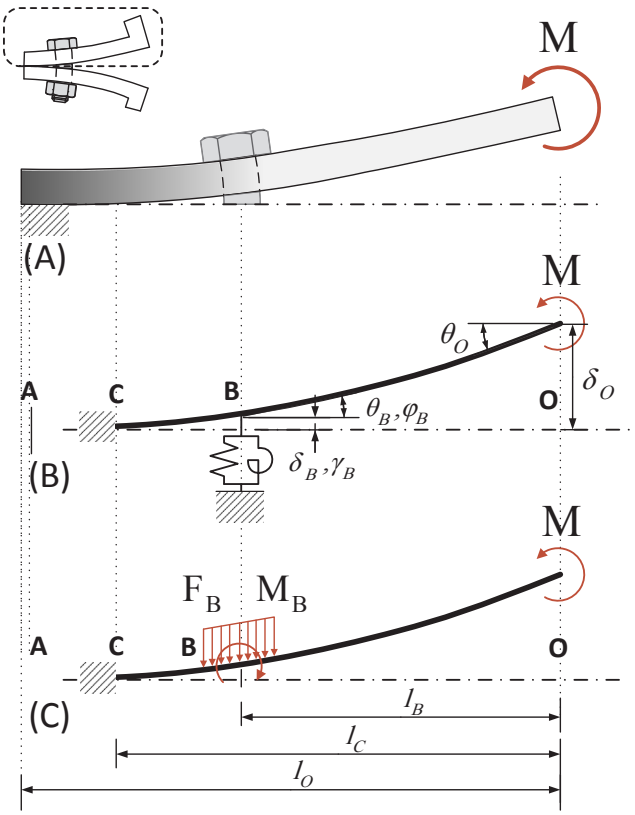

Fig. 3. Detailed of flange joint under positive moment, Flange lap (A), Equivalent model (B), Loading (C).

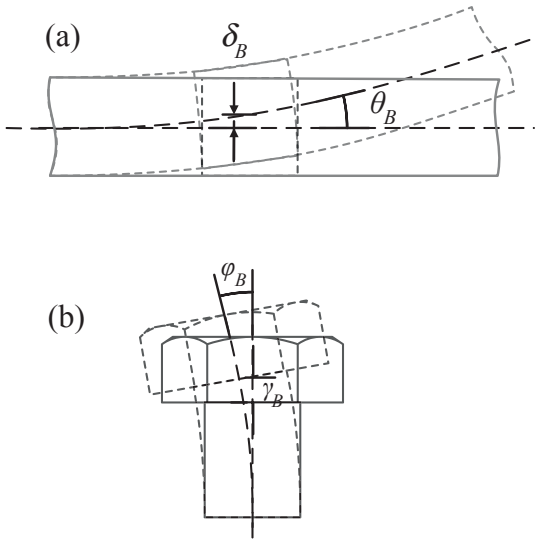

Fig. 4. Deformation and slope of (a) flange lap, (b) bolt.

separated length parameter (X), loadings (M, F_B, M_B) and other geometrical parameters of the model, the flange slope (θ_O^+) can be explicitly calculated with respect to external moment (M^+), which indicates the equivalent positive stiffness ($K_t{}^+$). So, we have:

$$K_t^+ = \frac{\theta_O^+}{M^+} \tag{5}$$

Detailed equations for calculating the unknown parameters are presented in Appendix A.

2.3.2. Negative deformations

Fig. 5-A shows a half joint model under negative bending moment. Similar to the positive loading, a beam-spring model is considered for studying mechanical behavior of the joint. The bolt presence is shown as distributed normal force and moment. Unlike the positive deformations, an axillary internal force F_O must be considered at point O, which is the 4th unknown variable. This force presents the internal interaction between two laps of the flange joint. It has been assumed that the flanges laps don't merge at point O.

The deflection and slope of the beam in case of the negative deformations (δ_B, δ_O and θ_B) are functions of the 4 unknown parameters X, F_O, F_B and M_B, where δ_O is the deflection of beam at point O. Similarly, three of the equations will be written similar to those presented for the positive deformation case (Eqs. (6)–(8)). In case of negative loading, see part (A) of Fig. 5, the lateral deflection of beam at point O is equal to zero. This condition can be used to derive the 4th equation (Eq. (9)) to find the 4th unknown variable.

$$F_O(X+1)l_B - F_B X l_B - M_B - M = 0 \tag{6}$$

$$\delta_B(F_B, M_B, F_O, X) = \gamma_B(F_B) \tag{7}$$

$$\theta_B(F_B, M_B, F_O, X) = \varphi_B(M_B) \tag{8}$$

$$\delta_O(F_B, M_B, F_O, X) = 0 \tag{9}$$

Solving Eqs. (6)–(9) leads to find four unknown variables (M, F_B, M_B and F_O). Having these unknown variables and other geometrical parameters of the model, the flange slope (θ_O^-) can be explicitly calculated with respect to external moment (M^-), which is the equivalent negative stiffness ($K_t{}^-$). So, we have:

$$K_t^- = \frac{\theta_O^-}{M^-} \tag{10}$$

Detailed equations for calculating the unknown parameters are presented in Appendix A.

2.4. Natural frequencies and mode shapes

In previous section it was shown that the equivalent stiffness of the joint has bilinear behavior (See Fig. 6). In this section, the mode shapes and natural frequencies of the beam-spring system are obtained. Then, putting two positive and negative stiffness in the equations leads to find separate mode shapes and frequencies. Dynamic behavior of the beam-spring system is piecewise linear in positive and negative deformations. Consequently, different natural frequencies and mode shapes will be obtained for positive and negative deformations. For this reason, two separate Euler-Bernoulli beam equations are considered (Eqs. (11-a) and (11-b)). These equations are used to present dynamic behavior of the beam 1 and 2, which are depicted in Fig. 2.

$$E_1 I_1 \frac{\partial^4 y_1}{\partial x_1^4} + \rho_1 A_1 \frac{\partial^2 y_1}{\partial t^2} = 0 \tag{11-a}$$

$$E_2 I_2 \frac{\partial^4 y_2}{\partial x_2^4} + \rho_2 A_2 \frac{\partial^2 y_2}{\partial t^2} = 0 \tag{11-b}$$

Using separation of variables technique and substituting $y(x, t) = Y(x)e^{i\omega t}$ into Eqs. (11), results in separating displacement dependent term from time dependent term. Note that, ω represents the natural frequency of transverse oscillation. The displacement dependent terms are presented as follows:

$$Y_1(x_1) = A_1 sin\beta_1 x_1 + B_1 cos\beta_1 x_1 + C_1 sinh\beta_1 x_1 + D_1 cosh\beta_1 x_1 \tag{12-a}$$

$$Y_2(x_2) = A_2 sin\beta_2 x_2 + B_2 cos\beta_2 x_2 + C_2 sinh\beta_2 x_2 + D_2 cosh\beta_2 x_2 \tag{12-b}$$

where β_1 and β_2 are presented as follows;

$$\beta_1^4 = \frac{\rho_1 A_1}{E_1 I_1}\omega^2 \quad \beta_2^4 = \frac{\rho_2 A_2}{E_2 I_2}\omega^2 \tag{13}$$

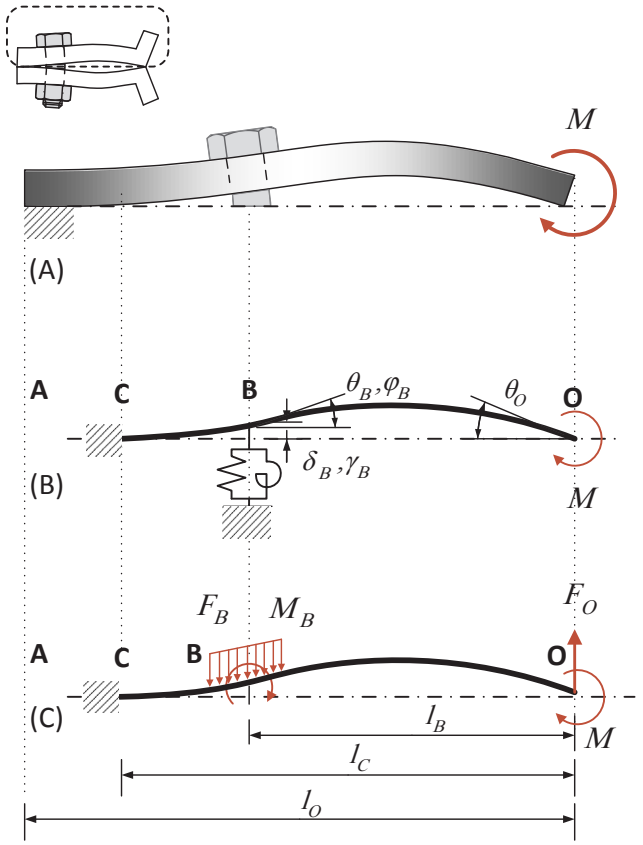

Fig. 5. Detailed of flange joint under negative moment, Flange lap (A), Equivalent model (B), Loading (C).

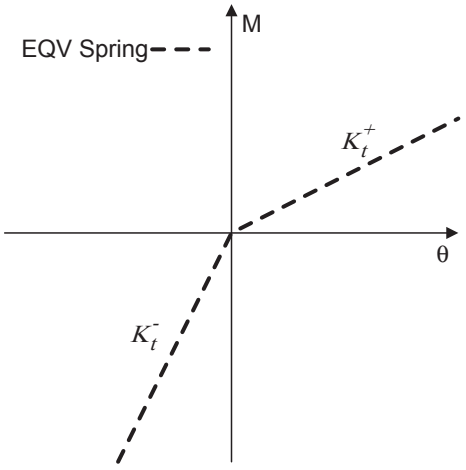

Fig. 6. Bilinear variation of external moment versus beam slope.

In this study, the free-free boundary condition is assumed for the system. Eight separate relations are given for boundary and compatibility conditions as shown in Eqs. (14-a)–(14-h).

$$\langle 1\rangle: \frac{d^2Y_1}{dx_1^2} = 0 \ at \ x_1 = 0 \tag{14-a}$$

$$\langle 2\rangle: \frac{d^3Y_1}{dx_1^3} = 0 \ at \ x_1 = 0 \tag{14-b}$$

$$\langle 3\rangle: \frac{d^2Y_2}{dx_2^2} = 0 \ at \ x_2 = L_2 \tag{14-c}$$

$$\langle 4\rangle: \frac{d^3Y_2}{dx_2^3} = 0 \ at \ x_2 = L_2 \tag{14-d}$$

$$\langle 5\rangle: Y_1|_{x_1=L_1} = Y_2|_{x_1=0} \tag{14-e}$$

$$\langle 6\rangle: E_1I_1\frac{d^3Y_1}{dx_1^3}\bigg|_{x_1=L_1} = E_2I_2\frac{d^3Y_2}{dx_2^3}\bigg|_{x_2=0} \tag{14-f}$$

$$\langle 7\rangle: \left\{\frac{dY_1}{dx_1}\bigg|_{x_1=L_1} - \frac{dY_2}{dx_2}\bigg|_{x_2=0}\right\}K_t = -E_1I_1\frac{d^2Y_1}{dx_1^2}\bigg|_{x_1=L_1} \tag{14-g}$$

$$\langle 8\rangle: \left\{\frac{dY_1}{dx_1}\bigg|_{x_1=L_1} - \frac{dY_2}{dx_2}\bigg|_{x_2=0}\right\}K_t = -E_2I_2\frac{d^2Y_2}{dx_2^2}\bigg|_{x_2=0} \tag{14-h}$$

Eight different equations will be obtained by substituting the boundary conditions into the governing equations of motion (Eqs. (12-a) and (12-b)). These equations are presented in terms of unknown coefficients A_1, B_1, C_1, D_1, A_2, B_2, C_2 and D_2. The equations are simplified and sorted with respect to the unknown variables as coefficient matrix in Appendix B. In order to extract the natural frequencies of the system, the eigenvalue solution can be used. Note that, in case of positive and negative deformations, different natural frequencies (ω^+ and ω^-) which are related to $K_t{}^+$ and $K_t{}^-$ will be obtained (see Eqs. (5) and (10)). Regarding physics of SDOF systems, they cannot have two fundamental natural frequencies. Time period of the free undamped vibration of bilinear oscillators can be obtained by averaging the time periods of ω^+ and ω^- [34] as is presented in Eq. (15).

$$T = \frac{T^+ + T^-}{2} \tag{15}$$

Replacing $T = 2\pi/\omega$, the natural frequency (ω) of the corresponding system is achieved as Eq. (16).

$$\omega = \frac{2\omega^+\omega^-}{\omega^+ + \omega^-} \tag{16}$$

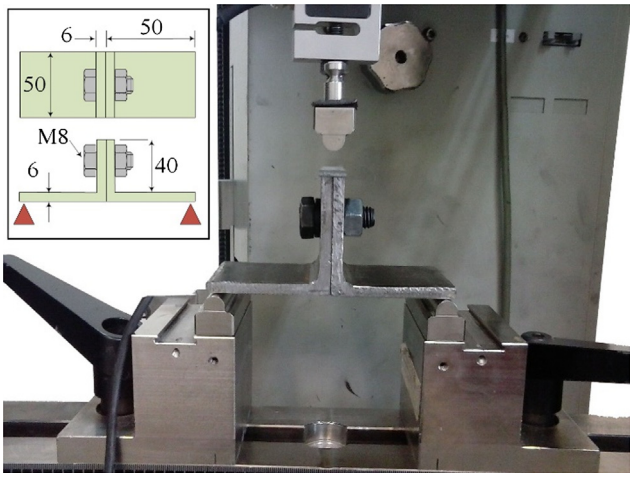

Fig. 7. Configuration and dimensions of the joint specimen embedded on the test device.

3. Experimental investigation

Two experimental setups have been developed in order to validate the proposed model of the flange joint and its analytical natural frequencies.

3.1. Static test

In order to validate the calculated flange stiffness results, obtained by analytical approach, an experimental setup including a single bolt steel flange joint was built. The bolt preload was tuned using an accurate torque meter. The test rig limitation does not allow enforcing only pure bending moment (As shown in Figs. 3 and 5) on the test specimen. So, a 3-point bending configuration was designed for the specimen enabling the investigation of bending behavior. Then the load deformation curves were extracted. The test was conducted using a Zwick Z250 universal testing machine. Fig. 7 shows the configuration and dimensions of the specimen under three-point flexural test.

The experiment procedure to find the force-deformation relationship, was designed to average the results obtained from five cycles of loading on a single specimen to avoid rising uncertainties due to changing specimens [35]. The specimen's flange was made of ST-37 steel and the bolt was from carbon steel with grade 8.8. During the tests, the applied load is controlled to avoid inelastic deformation of the specimen. Note that the maximum stress caused by the applied force during experiment, which is obtained using the FE model is equal to 175 MPa in flange and 156 MPa in the bolt, which are far from their yield strength [36].

3.2. Dynamic test

In this section, the experimental modal analysis (EMA) is performed on the vibratory system. A sample consisting of two beams connected by a single bolt flange joint was built for this purpose. Properties of the sample are presented in Table 3. System is excited by a modal hammer (Global Test AU-02) and the response is captured using an accelerometer (Global Test AP2037-100) at point 3. Fig. 8 shows the system subjected to modal hammer impulse excitation. The signal acquisition is performed with sampling rate 10 kHz, which is within the recommended frequency range [37]. The acceleration of separate impulse excitations at points 1–3 were measured and recorded. An average response of 5 impulses was calculated at each point to ensure coherence is as close as possible to the unity. A triangular impulse with 0.5 ms duration was generated as shown in Fig. 9. Hence, the frequency response functions are obtained as shown in Fig. 10.

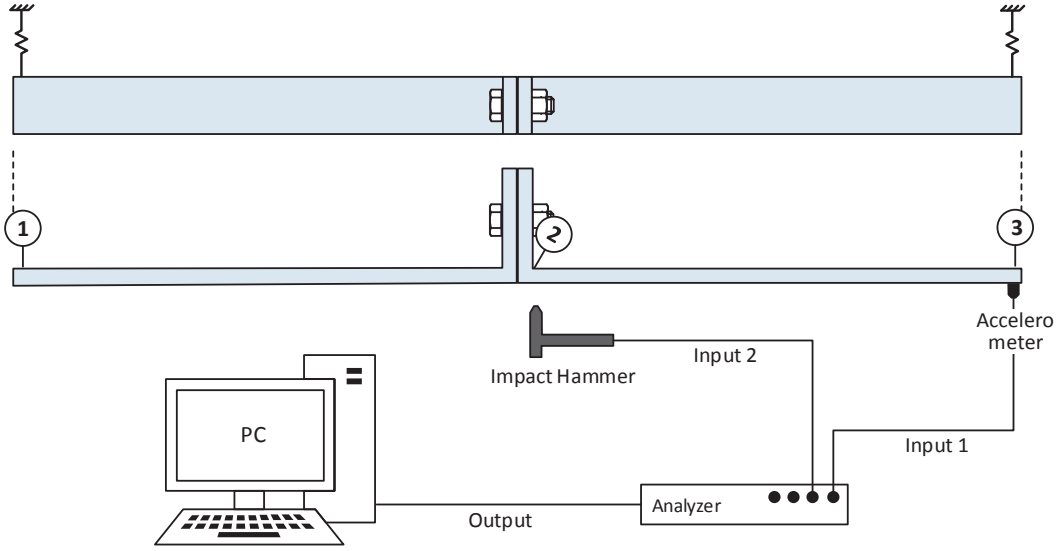

Fig. 8. Configuration of the impulse test.

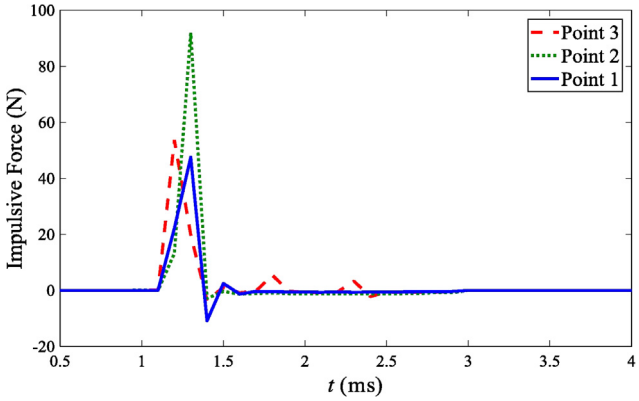

Fig. 9. Duration of the impulses.

Table 1
Properties of the supposed flange and bolt.

Parameter	Value	Parameter	Value
l_O (mm)	40	E_B (GPa)	200
l_B (mm)	27.5	I_B (mm^4)	201
I_{fl} (mm^4)	432	A_B (mm^2)	50.3
E_{fl} (GPa)	200	t_{fl} (mm)	6
$\nu_{fl,\ B}$	*0.3*	w_{fl} (mm)	50

4. Result comparison

4.1. Results of the flange stiffness

In this section, stiffness of the flange joint is calculated using the proposed procedure. Geometry and material properties of the assumed joint are listed in Table 1, which are selected regarding to the experiments carried out on the flange joint.

In order to evaluate the results of the proposed joint analytical model, finite element solution is obtained using ABAQUS software. Beam and bolt are modeled separately and assembled in the software. An elastic isotropic material with Young modulus $E = 200$ GPa, Poisson ratio $\nu = 0.3$ and density $\rho = 7800\ \mathrm{kg/m^3}$ is used. To obtain accurate result, the assembled system is meshed by employing the structural hexahedral elements [38]. Mesh refinement also carried out on the model to reach the optimum element size. Fig. 11 presents stress contour in flange lap and bolt's cross section. Then, predefined loading "bolt loads" is implemented to the model [38]. This loading exerts an internal tension force on the inner section of the bolt. Interaction between the joint laps is simulated considering surface to surface contact having finite sliding. The finite-sliding tracking approach allows for arbitrary separation, sliding, and rotation of the surfaces [38]. Isotropic friction with the coefficient of 0.6 is considered for tangential behavior of the contact [39]. The analysis is done by inserting external moment and setting appropriate boundary conditions.

Fig. 12 shows variations of beam slope with respect to external moment, which are obtained using data from finite element analysis, conducted experiments and the presented analytical method. It shows that the bending stiffness of the joint displays a bi-linear behavior with a single change at the equilibrium point. Stiffness of the positive loading (Opening moment) have lower value than the negative loading

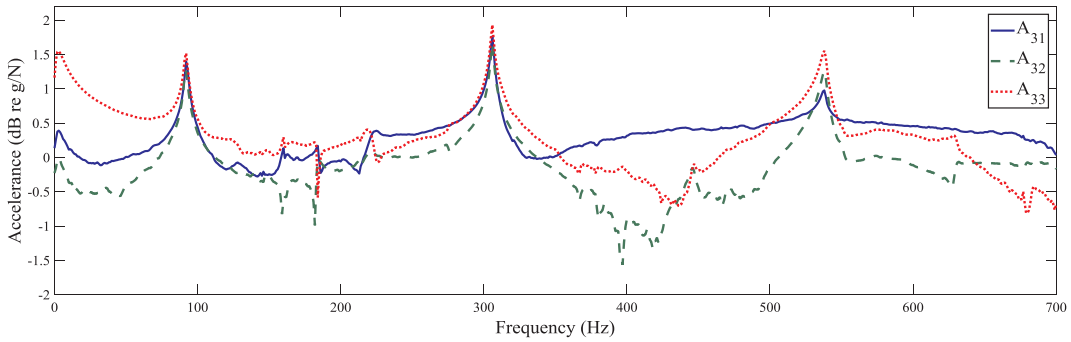

Fig. 10. Frequency response functions due to excitations in points 1–3.

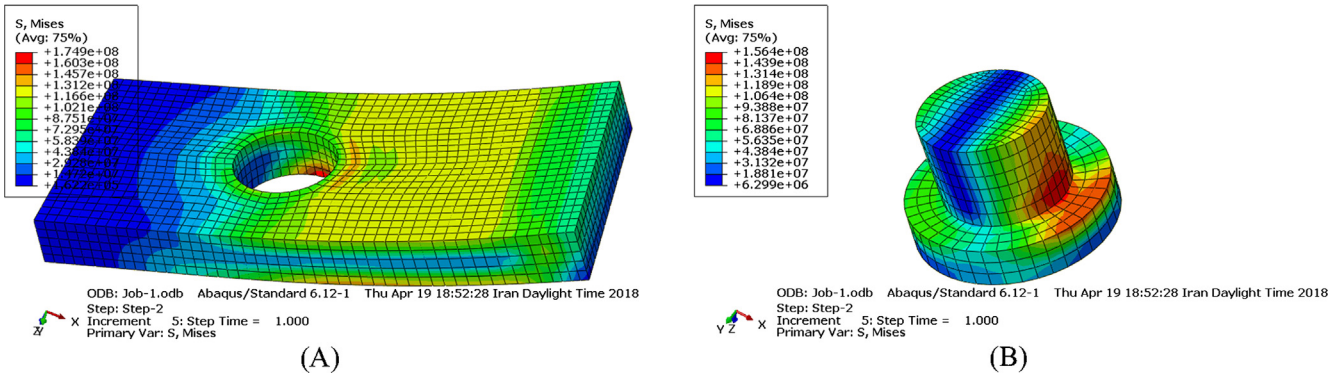

Fig. 11. Stress contour in flange lap (A) and bolt's cross section (B) under lateral loading.

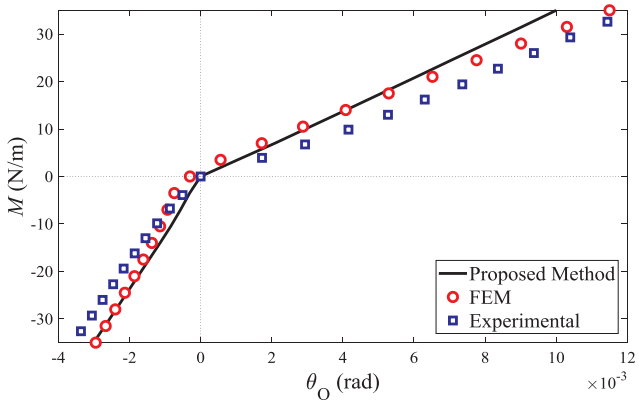

Fig. 12. Variation of the moment with respect to bending slope using the analytical method, FE and experiment.

Table 2
Comparison of the analytical, FEM and experimental stiffness.

Solution method	K_t^+ (kN.m/rad)	Error (%)	K_t^- (kN.m/rad)	Error (%)
Experimental	3.26	–	10.8	–
Analytical	3.54	8.59	11.2	3.70
FEM	3.07	5.83	11.5	6.48

(closing moment). In this comparison the bolt preload was set to 2000 N, and the external loading varied from −35 to +35 N.m. In high preloads separation of the flange laps will become so limited which cannot be detected by our experimental devices. Hence, the preload was set to 2000 N just to make the deflections detectable. In actual structures, this could be representation of a non-tightened bolt. The results, are shown in Table 2. The error was calculated based on the percent of difference between analytical (or FEM) and experimental divided by experimental results.

The differences observed between the above results may be due to the following reasons:

1- The analytical solution was obtained based on hypothetical geometry and material properties, which may not fit exactly to the actual system.
2- Limitations of the test rig to exert pure bending moment on the specimen.
3- Errors in data acquisition and finite element modeling.

4.2. Results of the equivalent Beam-Spring model

Table 4 shows three first natural frequencies of beam-spring system having characteristics shown in Table 3 for different joint stiffness. The first row represents closely the frequencies of the rigid joint. This was implemented by increasing the joint stiffness to very high orders. Theoretically, if the stiffness tends to infinity, the deflected beam, used to describe the joint laps, will be straight with constant slope. If two beams have the same sectional and material properties, the frequencies and the mode shapes would be equal to those of the continuous beams having a length of $L_1 + L_2$. Note that, the second natural frequency is not affected by the change in joint stiffness. The reason for this behavior is the fact that the joint is located at the node of the second mode of vibration. In this condition, the joint encounters no deformation and consequently the second natural frequencies remain constant. Fig. 13 shows the first mode shape of the system with respect to different joint stiffness. It can be seen that the discontinuity of the beam slop at the joint location increases with decrease in the joint stiffness.

A comparison of analytical (Section 2) and experimental results obtained from a system containing two beams, connected by a single bolt flange joint is carried out for the following reasons:

- To prove that the new proposed model can accurately calculate the stiffness of a single-bolt flange joint
- To prove that in beam-flange systems, replacing the flange joint configuration with an equivalent combination of two springs is justified.

Table 3
Characteristics of the beam-flange system (Fig. 2).

Parameter	Value	Parameter	Value
L_1, L_2	250 mm	M_f	0.3 kg
E_1, E_2	2×10^{11}	K_t^+	2.5×10^3
I_1, I_2	450 mm^4	K_t^-	3.5×10^3
ρ_1, ρ_2	7800 kg/m^3	K_l	5.0×10^7

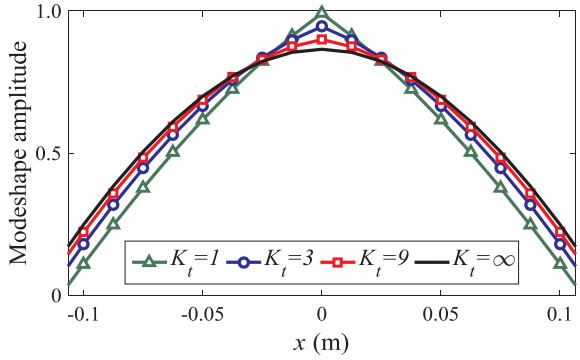

Fig. 13. First mode shape of the beam-flange system for different bending stiffness of the flange joint ($\times 10^3$).

Table 4
Natural frequencies of the beam-flange system for different bending stiffness of the flange joint.

Stiffness	f_1	f_2	f_3
$K_t \approx \infty$	109.3	343.7	584.8
$K_t = 9 \times 10^3$	103.1	343.7	552.6
$K_t = 3 \times 10^3$	93.3	343.7	513.0
$K_t = 1 \times 10^3$	74.8	343.7	463.5

Table 5
Comparison between natural frequencies of the proposed analytical model and experimental setup.

Linear frequencies ($f_i^{+,-}$) (Hz)	Analytical frequency (Hz)	Experimental frequency (Hz)	Error (%)
$f_1^+ = 90.7$ & $f_1^- = 95.1$	92.8	92	0.9
$f_2^+ = 343.7$ & $f_2^- = 343.7$	343.7	306	12.3
$f_3^+ = 504.8$ & $f_3^- = 519.7$	512.1	538	4.8

4.2.1. Natural frequencies

As shown in Section 2, the beam-flange system can be reduced to a nonlinear beam-spring system. Natural frequencies of the system, experimentally were measured and recorded then analytically calculated, using parameter values in Table 3. Table 5 compares the 3 first of these analytical and experimental natural frequencies of the system. Note that in this table, the analytical frequency is equal to $f_i = 2f_i^+ f_i^- / (f_i^+ + f_i^-)$ and it shows that there is a good agreement between the analytical and experimental results. Note that, bolted joints commonly have uncertainties which can affect the results [40]. The error was calculated based on the percent of difference between analytical and experimental divided by experimental results. However, the main sources of the shown errors are specified as follows:

- Experimental errors due to multiple causes such as, sample geometry and material, boundary conditions, test rig instruments (like hammer), sensors and also errors in exerting the impulse. etc.
- The difference between the actual beams with the assumed analytical model (based on Euler-Bernoulli beam theory).
- Errors caused by the location of excitation point. As stated before, placing the joint location at the node of the vibration mode shape in some frequencies causes disorders on data acquisition processes. In this case, the flange location is coincided with a node of the second mode shape.

5. Conclusions

In this study, a novel analytical model has been proposed for single bolt flange joints, which accurately simulates their dynamic behavior. In doing so, the joint laps and bolts are respectively modeled using the Euler-Bernoulli beams and combination of torsional and longitudinal springs. Then, a relation between external bending moment and slope of the beams is obtained and it is concluded that unlike the lap joints, the flange joints should be modeled using bilinear springs. Therefore, a new analytical formulation is introduced to precisely describe mechanical behavior of the flange joints. Static and dynamic behaviors of the joint are investigated using experimental prototypes. Comparing the theoretical results with the experimental and numerical results shows that the proposed model can accurately follow the experimental results. Especially for the stiffness in static loading, it is shown that error of the analytically obtained results is smaller than 8.59%. Furthermore, to ensure that the presented model can accurately describe the dynamic behavior of flange joints, the experimentally obtained natural frequencies are compared with the analytical results. It is shown that error of the fundamental frequency, which is calculated using the theoretical results, is smaller than 1%. Finally, it should be noted that the presented model for single bolt joints can easily be applicable for T-stab and endplate connections with little changes. Moreover, it should be noted that deriving the full model of a circular flange needs further assumptions and calculations, which should be considered in future studies.

Appendix A

Equations of deflection and slope of the flange laps are presented for positive and negative loadings as follows:

A.1. Positive loadings

Eqs. (A-1) and (A-2) shows deflection of flange lap and bolt at the bolt location l_B. Eqs. (A-3) and (A-4) also shows slope of flange lap and bolt at this location. Preload of the bolt is showed by F_{B0}.

$$\delta_B = \frac{(M+M_B)(Xl_B)^2}{2E_{fl}I_{fl}} - \frac{F_B/2R_B}{6E_{fl}I_{fl}}(Xl_B)^2 \int_{Xl_B}^{Xl_B+R_B}(3x-Xl_B)dx - \frac{F_B/2R_B}{6E_{fl}I_{fl}} \int_{Xl_B-R_B}^{Xl_B} x^2(3Xl_B-x)dx \tag{A-1}$$

$$\gamma_B = \frac{(F_B-F_{B0})t_{fl}}{E_B A_B} \tag{A-2}$$

$$\theta_B = \frac{(M+M_B)Xl_B}{E_{fl}I_{fl}} - \frac{F_B/2R_B}{2E_{fl}I_{fl}} Xl_B \int_{Xl_B}^{Xl_B+R_B}(2x-Xl_B)dx - \frac{F_B/2R_B}{2E_{fl}I_{fl}} \int_{Xl_B-R_B}^{Xl_B} x^2 dx \tag{A-3}$$

$$\varphi_B = \frac{M_B t_{fl}}{E_B I_B} \tag{A-4}$$

Eq. (A-5) represents three equations, which are respectively corresponded to deflections of beam at B, slopes at B and moment conservation.

Therefore, having the external loading, geometry and material of the system, the unknown parameters (X, M_B, F_B) can be found by solving three equations.

$$\begin{cases} \delta_B - \gamma_B = 0 \\ \theta_B - \varphi_B = 0 \\ M - M_B - F_B X l_B = 0 \end{cases} \tag{A-5}$$

Eq. (A-6) presents the slope of the flange lap at the load location under the external moment at this location. Note that, relationship between the slope of flange end and the external moment represents the flange stiffness under the positive loadings ($K_t{}^+$).

$$\theta_O = \frac{(M - M_B)(X+1) l_B}{E_{fl} I_{fl}} - \frac{F_B / 2R_B}{2E_{fl} I_{fl}} \int_{Xl_B - R_B}^{Xl_B + R_B} x^2 dx \tag{A-6}$$

A.2. Negative loadings

At this case of loadings, the equations of the bolt deflection and slope are same as the positive loadings. Deflection and slope of the flange lap at the bolt location l_B are respectively presented in Eqs. (A-7) and (A-8). Eq. (A-9) also shows deflection of the flange end (point O in Fig. 5).

$$\delta_B = \frac{F_O X^2 (2X + 3) l_B^3}{6E_{fl} I_{fl}} - \frac{(M + M_B)(Xl_B)^2}{2E_{fl} I_{fl}} - \frac{F_B / 2R_B}{6E_{fl} I_{fl}} (Xl_B)^2 \int_{Xl_B}^{Xl_B + R_B} (3x - Xl_B) dx - \frac{F_B / 2R_B}{6E_{fl} I_{fl}} \int_{Xl_B - R_B}^{Xl_B} x^2 (3Xl_B - x) dx \tag{A-7}$$

$$\theta_B = \frac{F_O X (X+2) l_B^2}{2E_{fl} I_{fl}} - \frac{(M + M_B) Xl_B}{E_{fl} I_{fl}} - \frac{F_B / 2R_B}{2E_{fl} I_{fl}} Xl_B \int_{Xl_B}^{Xl_B + R_B} (2x - Xl_B) dx - \frac{F_B / 2R_B}{2E_{fl} I_{fl}} \int_{Xl_B - R_B}^{Xl_B} x^2 dx \tag{A-8}$$

$$\delta_O = \frac{F_O (X+1)^3 l_B^3}{3E_{fl} I_{fl}} - \frac{M (X+1)^2 l_B^2}{2E_{fl} I_{fl}} - \frac{M_B (Xl_B)^2 (X+2)}{2E_{fl} I_{fl}} - \frac{F_B / 2R_B}{6E_{fl} I_{fl}} \int_{Xl_B - R_B}^{Xl_B + R_B} x^2 (3Xl_B + 3l_B - x) dx \tag{A-9}$$

Eq. (A-10) represents four equations, which are respectively corresponded to moment conservation, deflections at B, slope at B and deflection at C. Therefore, Having the external loading, geometry and material of the system, the unknown parameters (X, M_B, F_B, F_O) can be found by solving four equations.

$$\begin{cases} F_O (X+1) l_B - M_B - M - F_B X l_B = 0 \\ \delta_B - \gamma_B = 0 \\ \theta_B - \varphi_B = 0 \\ \delta_O = 0 \end{cases} \tag{A-10}$$

Eq. (A-11) presents the slope of the flange lap at the load location (O) under the external moment at O. Note that, in case of the negative loadings, relationship between the slope of flange end and the external moment represents the negative flange stiffness ($K_t{}^-$).

$$\theta_O = \frac{F_O (X+1)^3 l_B^3}{3E_{fl} I_{fl}} - \frac{(M + M_B)(X+1) l_B}{E_{fl} I_{fl}} - \frac{F_B / 2R_B}{2E_{fl} I_{fl}} \int_{Xl_B - R_B}^{Xl_B + R_B} x^2 dx \tag{A-11}$$

Appendix B

Eigen matrix is shown as follow equation:

$$K = \begin{bmatrix} 0 & 1 & 0 & -1 & 0 & 0 & 0 & 0 \\ 1 & 0 & -1 & 0 & 0 & 0 & 0 & 0 \\ 0 & 0 & 0 & 0 & s(\beta_2 L_2) & c(\beta_2 L_2) & -sh(\beta_2 L_2) & -ch(\beta_2 L_2) \\ 0 & 0 & 0 & 0 & -c(\beta_2 L_2) & s(\beta_2 L_2) & ch(\beta_2 L_2) & sh(\beta_2 L_2) \\ s(\beta_1 L_1) & c(\beta_1 L_1) & sh(\beta_1 L_1) & ch(\beta_1 L_1) & 0 & -1 & 0 & -1 \\ \beta_1^3 \varnothing c(\beta_1 L_1) & -\beta_1^3 \varnothing s(\beta_1 L_1) & -\beta_1^3 \varnothing ch(\beta_1 L_1) & -\beta_1^3 \varnothing sh(\beta_1 L_1) & -\beta_2^3 & 0 & -\beta_2^3 & 0 \\ [K_t \beta_1 c(\beta_1 L_1) - \beta_1^2 E_1 I_1 s(\beta_1 L_1)] & [-K_t \beta_1 s(\beta_1 L_1) & [K_t \beta_1 ch(\beta_1 L_1) & [K_t \beta_1 sh(\beta_1 L_1) & -K_t(\beta_2) & 0 & -K_t(\beta_2) & 0 \\ & -\beta_1^2 E_1 I_1 c(\beta_1 L_1)] & + \beta_1^2 E_1 I_1 sh(\beta_1 L_1)] & + \beta_1^2 E_1 I_1 ch(\beta_1 L_1)] & & & & \\ K_t \beta_1 c(\beta_1 L_1) & -K_t \beta_1 s(\beta_1 L_1) & K_t \beta_1 ch(\beta_1 L_1) & K_t \beta_1 sh(\beta_1 L_1) & -K_t(\beta_2) & -\beta_2^2 (E_2 I_2) & -K_t(\beta_2) & \beta_2^2 (E_2 I_2) \end{bmatrix}$$

References

[1] Dubina D, Ungureanu V. Behaviour of multi-span cold-formed Z-purlins with bolted lapped connections. Thin-Walled Struct 2010;48(10):866–71.

[2] Keerthan P, Hughes D, Mahendran M. Experimental studies of hollow flange channel beams subject to combined bending and shear actions. Thin-Walled Struct 2014;77(Supplement C):129–40.

[3] Blachowski B, Gutkowski W. Effect of damaged circular flange-bolted connections on behaviour of tall towers, modelled by multilevel substructuring. Eng Struct 2016;111(Supplement C):93–103.

[4] Cheng S, Becque J. A design methodology for side wall failure of RHS truss X-joints accounting for compressive chord pre-load. Eng Struct 2016;126(Supplement C):689–702.

[5] Morohoshi T, Sawa T. On the characteristics of rectangular bolted flanged connections with gaskets subjected to external tensile loads and bending moments. J Pressure Vessel Technol 1994;116(2):207–15.

[6] Schwingshackl CW, et al. Modeling and validation of the nonlinear dynamic

behavior of bolted flange joints. J Eng Gas Turbines Power 2013;135(12). 122504 122504.
[7] Law SS, Wu ZM, Chan SL. Vibration control study of a suspension footbridge using hybrid slotted bolted connection elements. Eng Struct 2004;26(1):107–16.
[8] de Benedetti M, et al. On the damping effect due to bolted junctions in space structures subjected to pyro-shock. Acta Astronaut 2007;60(12):947–56.
[9] Zapico-Valle JL, et al. Modelling and calibration of a beam-column joint based on modal data. Comput Struct 2012;108–109:31–41.
[10] Rezaee MS, et al. Stability of a system consisting of three-axis connected through Hooke's joints. Modares Mech Eng 2013;12(6):69–79.
[11] Di Maio D, Schwingshackl C, Sever IA. Development of a test planning methodology for performing experimental model validation of bolted flanges. Nonlinear Dyn 2016;83(1):983–1002.
[12] Semke WH, et al. Efficient dynamic structural response modelling of bolted flange piping systems. Int J Press Vessels Pip 2006;83(10):767–76.
[13] Abad J, Medel FJ, Franco JM. Determination of Valanis model parameters in a bolted lap joint: Experimental and numerical analyses of frictional dissipation. Int J Mech Sci 2014;89:289–98.
[14] Guo Y, et al. Nonlinearity of interfaces and force transmission of bolted flange joints under impact loading. Int J Impact Eng 2017;109(Supplement C):214–23.
[15] Hwang DY, Stallings JM. Finite element analysis of bolted flange connections. Comput Struct 1994;51(5):521–33.
[16] Wang M, Wang D, Zheng G. Joint dynamic properties identification with partially measured frequency response function. Mech Syst Sig Process 2012;27:499–512.
[17] Hantouche EG, et al. Modified stiffness model for thick flange in built-up T-stub connections. J Constr Steel Res 2013;81:76–85.
[18] Wu Z, Nassar SA, Yang X. Nonlinear deformation behavior of bolted flanges under tensile, torsional, and bending loads. J Pressure Vessel Technol 2014;136(6). 061201 061201.
[19] Zhu L, Bouzid A-H, Hong J. Numerical and experimental study of elastic interaction in bolted flange joints. J Pressure Vessel Technol 2017;139(2). pp. 021211–021211-7.
[20] Lavassas I, et al. Analysis and design of the prototype of a steel 1-MW wind turbine tower. Eng Struct 2003;25(8):1097–106.
[21] Lee S-Y, Ko K-H, Lee J. Analysis of dynamic characteristics of structural joints using stiffness influence coefficients. KSME Int J 2000;14(12):1319–27.
[22] Agatonovic P. Beam model of bolted flanged connections. Eng Comput 1985;2(1):21–9.
[23] Shi Y, Chan S, Wong Y. Modeling for moment-rotation characteristics for end-plate connections. J Struct Eng 1996;122(11):1300–6.
[24] Luan Y, et al. A simplified nonlinear dynamic model for the analysis of pipe structures with bolted flange joints. J Sound Vib 2012;331(2):325–44.
[25] Meisami F, et al. Analytical and experimental investigation for nonlinear behavior of flange joints under axial and lateral loading. J. Solid Fluid Mech 2016;6(3):43–54.
[26] Tanaka M. The stress analysis of bolted joint with model using spring-beam elements-a case of T-flange joint. J Jpn Soc Precision Eng 1988;54(2):323.
[27] Sawa T, Morohoshi T, Yamamoto K. A stress analysis of pipe flange connections subjected to external bending moments. Pergamon; 1989. p. 501–8.
[28] Abid M, Nash DH. Structural strength: Gasketed vs non-gasketed flange joint under bolt up and operating condition. Int J Solids Struct 2006;43(14–15):4616–29.
[29] Swanson J, Leon R. Stiffness modeling of bolted T-stub connection components. J Struct Eng 2001;127(5):498–505.
[30] Ahmadian H, Jalali H. Identification of bolted lap joints parameters in assembled structures. Mech Syst Sig Process 2007;21(2):1041–50.
[31] Ahmadian H, Jalali H. Generic element formulation for modelling bolted lap joints. Mech Syst Sig Process 2007;21(5):2318–34.
[32] Jalali H, Ahmadian H, Mottershead JE. Identification of nonlinear bolted lap-joint parameters by force-state mapping. Int J Solids Struct 2007;44(25–26):8087–105.
[33] Iranzad M, Ahmadian H. Identification of nonlinear bolted lap joint models. Comput Struct 2012;96–97:1–8.
[34] Peng ZK, et al. Analysis of bilinear oscillators under harmonic loading using non-linear output frequency response functions. Int J Mech Sci 2007;49(11):1213–25.
[35] Ibrahim RA, Pettit CL. Uncertainties and dynamic problems of bolted joints and other fasteners. J Sound Vib 2005;279(3–5):857–936.
[36] Shigley J, Mischke C. Mechanical engineering design. 7th ed. Elizabeth A. Jones; 2004.
[37] GlobalTest. AP2037-100 Accelerometer Catalog; 2017: http://globaltest.ru/ru/gt_product/ap2037-100/.
[38] Simulia, D.S., Abaqus 6.12 documentation. Providence, Rhode Island, US, 2012.
[39] Sullivan JF. Technical physics. Wiley; 1988.
[40] Ibrahim RA, Pettit CL. Uncertainties and dynamic problems of bolted joints and other fasteners. J Sound Vib 2005;279(3):857–936.